Visualizing revivals and fractional revivals in a Kerr medium using an optical tomogram

M. Rohith and C. Sudheesh
Department of Physics, Indian Institute of Space Science and Technology, Thiruvananthapuram 695 547, India
(Received 14 July 2015; published 11 November 2015)

We study theoretically optical tomograms of the time-evolved states generated by the evolution of different kinds of initial wave packets in a Kerr medium. An exact analytical expression for the optical tomogram of the quantum state at any instant during the evolution of a generic initial wave packet is derived in terms of Hermite polynomials. The time evolution of the optical tomogram is discussed for three kinds of initial states: a coherent state, an m-photon-added coherent state, and even and odd coherent states. We show the manifestation of revival and fractional revivals in the optical tomograms of the time-evolved states. We find that the optical tomogram of the time-evolved state at the instants of fractional revivals shows structures with sinusoidal strands. The number of sinusoidal strands in the optical tomogram of the time-evolved state at l-subpacket fractional revivals is l times the number of sinusoidal strands present in the optical tomogram of the initial state. We also investigate the effect of decoherence on the optical tomograms of the states at the instants of fractional revivals for the initial states considered above. We consider amplitude decay and phase damping models of decoherence and show the direct manifestations of decoherence in the optical tomogram.

DOI: 10.1103/PhysRevA.92.053828 PACS number(s): 42.50.Dv, 03.65.Wj, 42.50.Md

I. INTRODUCTION

The time evolution of an initial wave packet in a nonlinear medium can exhibit revival and fractional revivals at specific instants of time. The revival phenomenon has been investigated both theoretically and experimentally in a wide class of systems [1]. A revival of a well-localized initial wave packet occurs when it evolves in time to a wave packet that reproduces the initial waveform. The characteristic time scale over which this phenomenon happens is called the revival time $T_{\rm rev}$. Within this characteristic time scale $T_{\rm rev}$, the wave packet may split into a number of scaled copies of the initial state at specific instants during the evolution. This is known as the fractional revival of the initial wave packets [2]. An l-subpacket fractional revival occurs when the initial wave packet splits into a superposition of l wave packets of the initial form. The revivals and fractional revival have been observed experimentally in a variety of quantum systems such as Rydberg atomic wave packets, molecular vibrational states, Bose-Einstein condensates, and so forth [3–9]. Fractional revivals occurring in a nonlinear medium can be used to generate various kinds of macroscopic superposition states of light. Such superposed states of light have potential applications in quantum optics and quantum information. The generation of a discrete superposition of coherent states at fractional revival times in the process of wave-packet propagation in a nonlinear medium was discussed in [10–13]. It has been shown that the superposed wave packets generated at fractional revival times, using an initial coherent state in a nonlinear medium, have application in quantum cloning [14]. Two and four superposition states generated at fractional revival instances are useful for implementing the one- and two-bit logic gates [15]. Recent experimental observation of multicomponent Schrödinger cat states using the single-photon Kerr effect opens up new directions for continuous-variable quantum computation [16].

The signatures of fractional revivals in the time evolution of various physical quantities have been investigated theoretically [17–23]. The experimental characterization of time-evolved states in a nonlinear medium is an important aspect in the study of revival and fractional revivals and it can be done by optical tomography, which is an efficient technique to measure and reconstruct the quantum state of optical fields [24]. Optical tomography is based on the one-to-one correspondence between the quasiprobability distribution and the probability distribution of rotated quadrature phases of the field [25]. The optical tomogram contains all the information about the system and can serve as an alternative representation of the quantum system, apart from the conventional state vector or its density-matrix representation in the appropriate Hilbert space. The optical tomogram of a quantum state can be calculated theoretically using a suitable transformation in the symplectic tomogram [26–32] of the quantum state. In fact, an alternative formulation of quantum mechanics in which the quantum states are described by tomographic probability distributions was suggested in [33]. In experiments, a series of homodyne measurements of the rotated quadrature operator of the field is done on an ensemble of identically prepared systems. The quadrature histogram obtained by this method is called an optical tomogram. The first experimental observation of the squeezed state of light, by measuring the quadrature amplitude distribution using the balanced homodyne detection arrangement, was made in [34]. Thereafter, many nonclassical states of light have been characterized by optical homodyne tomography. A review of continuous-variable optical quantum state tomography, including a list of the optical quantum states characterized by the same, is given in [35].

It is a usual practice in experiments to reconstruct the density matrix or the quasiprobability distributions of the system from the optical tomogram and study its nonclassical properties. The reconstructed quasiprobability distributions, such as the Wigner function and Husimi Q function, provide a convenient way to visualize the fractional revivals in phase space. Recently, the quantum state collapse and revival due to the single-photon Kerr effect have been observed using a three-dimensional circuit quantum electrodynamic architecture and the multicomponent Schrödinger cat states generated at fractional revival times are visualized in phase

space using the quasiprobability distributions reconstructed from the optical tomogram [16]. It should be emphasized that no reconstruction process is perfect and the original errors of the experimental data can grow during the process of reconstruction. The physical properties of quantum states can be studied directly using an optical tomogram and the tomographic approach can be used to estimate the errors in the histograms of experimentally obtained quadrature values [36]. The macroscopic superposition states generated at the instants of fractional revivals are sensitive to interaction with their environment in an actual experimental setting; this interaction can even destroy the states generated. The aim of this paper is twofold: first, to find the signatures of revivals and fractional revivals directly in the optical tomogram, which in turn can help experimentalists avoid the errors that can accumulate during the reconstruction process, and second, to study the effects of amplitude decay and phase damping models of decoherence on the optical tomogram of the states at the instants of fractional revivals. For this purpose, we consider a nonlinear medium, which models the wave-packet propagation in a Kerr-like medium [37,38] and the dynamics of Bose-Einstein condensates [8]. This paper is organized as follows. In Sec. II we give a brief review of the tomographic representation of a quantum system. In Sec. III we calculate theoretically the optical tomogram of the time-evolved states in the nonlinear medium. Here we discuss the evolution of the optical tomogram for three specific initial states, which are a coherent state, an m-photon-added coherent state, and even and odd coherent states. Section IV describes the effect of amplitude loss and phase noise on the optical tomograms of the states at the instants of fractional revivals. In Sec. V we summarize the main results of this paper.

II. TOMOGRAPHIC REPRESENTATION OF THE QUANTUM STATE

Optical tomograms of several nonclassical states of light have been investigated theoretically in the literature [39–42]. A brief discussion about the calculation of the optical tomogram of a quantum state and the general properties of the optical tomogram is given below. Consider the homodyne quadrature operator

$$\hat{X}_\theta = \frac{1}{\sqrt{2}}(ae^{-i\theta} + a^\dagger e^{i\theta}), \tag{1}$$

where θ is the phase of the local oscillator in the homodyne detection setup and a and $a^\dagger$ are the photon annihilation and creation operators of the single-mode electromagnetic field, respectively. The phase of the local oscillator varies in the domain $0 \leqslant \theta \leqslant 2\pi$. The optical tomogram $\omega(X_\theta,\theta)$ of a quantum state with density matrix ρ can be calculated by the following expression [25,35]:

$$\omega(X_\theta,\theta) = \langle X_\theta,\theta|\rho|X_\theta,\theta\rangle, \tag{2}$$

where

$$|X_\theta,\theta\rangle = \frac{1}{\pi^{1/4}} \exp\left[-\frac{{X_\theta}^2}{2} - \frac{1}{2}e^{i2\theta}a^{\dagger 2} + \sqrt{2}e^{i\theta}X_\theta a^\dagger\right]|0\rangle$$

is the eigenvector of the Hermitian operator $\hat{X}_\theta$ with eigenvalue X_θ [43]. For a pure quantum state with wave vector $|\psi\rangle$, the expression (2) can be rewritten as

$$\omega(X_\theta,\theta) = |\langle X_\theta,\theta|\psi\rangle|^2. \tag{3}$$

The normalization condition of the optical tomogram $\omega(X_\theta,\theta)$ is given by

$$\int dX_\theta \omega(X_\theta,\theta) = 1. \tag{4}$$

The optical tomogram $\omega(X_\theta,\theta)$ of a quantum state is nonnegative and has the following symmetry property:

$$\omega(X_\theta,\theta+\pi) = \omega(-X_\theta,\theta). \tag{5}$$

In the following sections we use Eq. (2) to evaluate the optical tomogram of the quantum states generated by the Kerr medium.

III. OPTICAL TOMOGRAMS OF STATES GENERATED IN A NONLINEAR MEDIUM

Consider the dynamics of a single-mode field governed by a nonlinear Hamiltonian

$$H = \hbar\chi a^{\dagger 2}a^2 = \hbar\chi N(N-1), \tag{6}$$

where a and $a^\dagger$ are the photon annihilation and creation operators, respectively. The eigenstates of the operator $N = a^\dagger a$ are the Fock states $|n\rangle$, where $n = 0,1,2,\ldots,\infty$. The positive constant χ merely sets the time scale in the problem. We choose the numerical value of χ to be 5 throughout this paper. Consider a general initial wave packet $|\psi(0)\rangle$, with its Fock state expansion

$$|\psi(0)\rangle = \sum_{n=0}^{\infty} C_n|n\rangle, \tag{7}$$

where C_n are the Fock state expansion coefficients. The time evolution of the state is governed by the Schrödinger equation

$$|\psi(t)\rangle = U(t)|\psi(0)\rangle, \tag{8}$$

where $U(t) = \exp[-iHt/\hbar]$ is the unitary time-evolution operator. The time-evolved state at time t can be written as

$$|\psi(t)\rangle = \sum_{n=0}^{\infty} C_n e^{-i\chi tn(n-1)}|n\rangle. \tag{9}$$

We calculate theoretically the optical tomogram of the time-evolved state $|\psi(t)\rangle$ and look for the signatures of revival and fractional revival in the optical tomogram. Inserting Eq. (9) in Eq. (3), we get the optical tomogram of the time-evolved state $|\psi(t)\rangle$ as

$$\omega(X_\theta,\theta,t) = \frac{e^{-X_\theta^2}}{\sqrt{\pi}}\left|\sum_{n=0}^{\infty}\frac{C_n e^{-i\chi tn(n-1)}}{\sqrt{n!}2^{n/2}}e^{-in\theta}H_n(X_\theta)\right|^2, \tag{10}$$

where $H_n(\cdot)$ denotes the Hermite polynomial of order n. Equation (10) gives the time evolution of the optical tomogram for an initial wave packet $|\psi(0)\rangle$ in a nonlinear medium modeled by the Hamiltonian H. In the following sections we discuss the temporal evolution of the optical tomogram for three different kinds of initial states, namely, a coherent state, an m-photon-added coherent state, and even and odd coherent states.

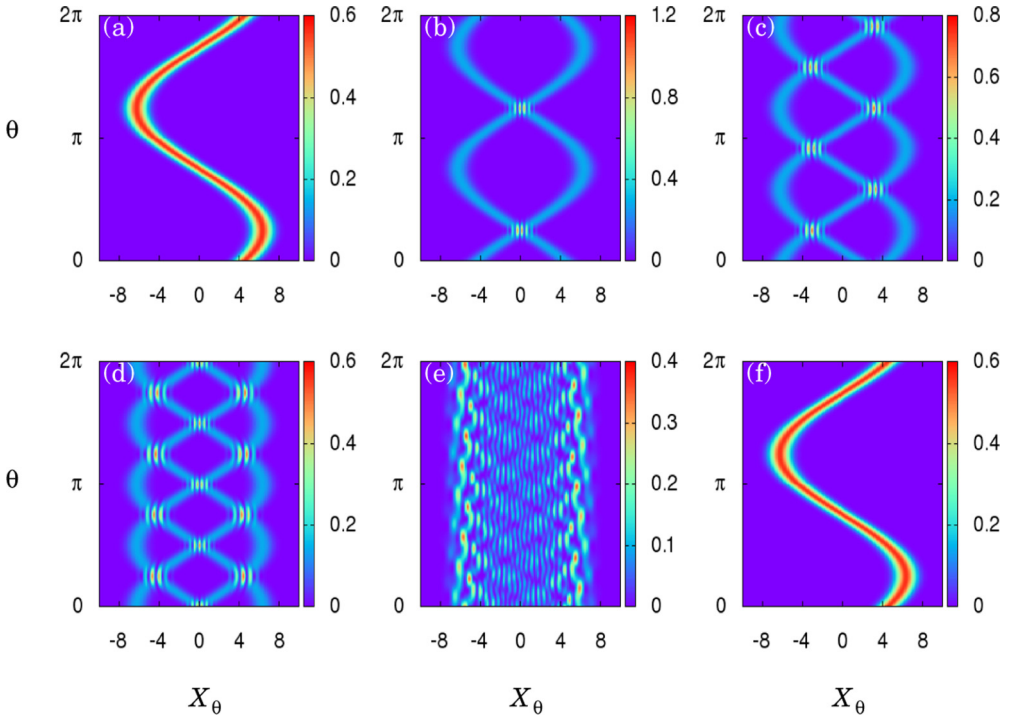

FIG. 1. (Color online) Time-evolved optical tomogram $\omega_\alpha(X_\theta,\theta,t)$ for an initial coherent state $|\alpha\rangle$ at (a) $t = 0$, (b) $t = T_{\rm rev}/2$, (c) $t = T_{\rm rev}/3$, (d) $t = T_{\rm rev}/4$, (e) $t = T_{\rm rev}/\sqrt{2}$, and (f) $T_{\rm rev}$, with field strength $|\alpha|^2 = 20$. At an l-subpacket fractional revival time $t = \pi/l\chi$, the optical tomogram of the state shows structures with l sinusoidal strands. The structures with sinusoidal strands are completely absent in the optical tomogram for the collapsed state at time $t = T_{\rm rev}/\sqrt{2}$.

A. Evolution of the coherent state

Consider the evolution of an initial coherent state $|\alpha\rangle$ in the nonlinear medium governed by the Hamiltonian in Eq. (6). The Fock state expansion coefficient C_n in Eq. (7) for the coherent state is

$$C_n = e^{-|\alpha|^2}\frac{\alpha^n}{\sqrt{n!}}. \tag{11}$$

Let $\alpha = \sqrt{|\alpha|^2}\exp(i\delta)$, where $|\alpha|^2$ is the mean number of photons in the coherent state $|\alpha\rangle$ and δ is a real number. Without loss of generality, we set $\delta = \pi/4$. Figure 1(a) displays the optical tomogram of the coherent state $|\alpha\rangle$ (at time $t = 0$), for which the optical tomogram is given by

$$\omega_\alpha(X_\theta,\theta,t=0) = \frac{1}{\sqrt{\pi}}\exp\{-[X_\theta - \sqrt{2}|\alpha|\cos(\delta-\theta)]^2\}. \tag{12}$$

The maximum intensity of this optical tomogram $\omega_\alpha(X_\theta,\theta,t = 0)$ is $1/\sqrt{\pi}$, which occurs along the sinusoidal path, defined by $X_\theta = \sqrt{2|\alpha|^2}\cos(\theta-\delta)$, in the X_θ-θ plane. Hence, the projection of the optical tomogram on the X_θ-θ plane is a structure with a single sinusoidal strand. Along the X_θ axis ($\theta = 0$), the maximum intensity of the optical tomogram occurs at $X_\theta = \sqrt{2|\alpha|^2}\cos\delta$.

The optical tomogram of the state at any instant during the evolution of a coherent state $|\alpha\rangle$ is calculated using Eq. (10):

$$\omega_\alpha(X_\theta,\theta,t) = \frac{e^{-|\alpha|^2}e^{-X_\theta^2}}{\sqrt{\pi}}\left|\sum_{n=0}^{\infty}\frac{\alpha^n e^{-i\chi t n(n-1)}}{n!2^{n/2}}e^{-in\theta}H_n(X_\theta)\right|^2. \tag{13}$$

Now we analyze the optical tomogram $\omega_\alpha(X_\theta,\theta,t)$ at the instants of fractional revivals. Between $t = 0$ and $t = T_{\rm rev}$, for an initial coherent state, l-subpacket fractional revivals occur at time $t = \pi j/l\chi$, where $j = 1,2,\ldots,l-1$ for a given value of l (>1) with the condition that j and l are mutually prime integers. Without loss of generality, we take $j = 1$. The analysis shown below is true for any possible value of j. The interesting periodicity properties of the unitary time evolution operator U in Eq. (8) at the instants of l-subpacket fractional revivals, that is, at times $t = \pi/l\chi$, enable us to write the time-evolved state $|\psi(t)\rangle$ at these instants as

$$\begin{aligned}|\psi_l\rangle &= |\psi(\pi/l\chi)\rangle \\ &= \begin{cases}\sum_{r=0}^{l-1} f_r^{(o)}|\alpha e^{-i2\pi r/l}\rangle & \text{if } l \text{ is odd} \\ \sum_{r=0}^{l-1} f_r^{(e)}|\alpha e^{-i\pi(2r-1)/l}\rangle & \text{if } l \text{ is even,}\end{cases}\end{aligned} \tag{14}$$

where

$$f_r^{(o)} = \frac{1}{l}\sum_{k=0}^{l-1}\exp\left[\frac{2\pi i r}{l}k\right]\exp\left[-\frac{i\pi}{l}k(k-1)\right], \tag{15}$$

$$f_r^{(e)} = \frac{1}{l}\sum_{k=0}^{l-1}\exp\left[\frac{2\pi i r}{l}k\right]\exp\left[-\frac{i\pi}{l}k^2\right] \tag{16}$$

are the Fourier coefficients [13]. Note that each of the ket vectors in Eq. (14) is a coherent state and hence the state $|\psi_l\rangle$ is a superposition of l coherent states. At an l-subpacket fractional revival time $t = \pi/l\chi$, Eq. (13) can be simplified to get the optical tomogram of the state $|\psi_l\rangle$ as

$$\omega_\alpha(X_\theta,\theta,t=\pi/l\chi) = \frac{1}{\sqrt{\pi}}\left|\sum_{r=0}^{l-1} f_{r,l}\exp\left[-\frac{X_\theta^2}{2}-\frac{|\alpha|^2}{2}-\frac{\alpha_{r,l}^2 e^{-i2\theta}}{2} + \sqrt{2}\alpha_{r,l}X_\theta e^{-i\theta}\right]\right|^2, \tag{17}$$

where

$$f_{r,l} = \begin{cases} f_r^{(o)} & \text{if } l \text{ is odd} \\ f_r^{(e)} & \text{if } l \text{ is even,} \end{cases}$$
$$\alpha_{r,l} = \begin{cases} \alpha e^{-i2\pi r/l} & \text{if } l \text{ is odd} \\ \alpha e^{-i\pi(2r-1)/l} & \text{if } l \text{ is even.} \end{cases} \tag{18}$$

Figures 1(b)–1(d), show the optical tomograms of the state $|\psi_l\rangle$ for $l = 2$, 3, and 4, corresponding to the two-, three-, and four-subpacket fractional revivals of the initial coherent state, respectively. The value of the field strength $|\alpha|^2$ used to plot the tomograms in the figures is 20. Figure 1(b) shows the optical tomogram of the state $|\psi_2\rangle$, which is the superposition of the coherent states $|i\alpha\rangle$ and $|-i\alpha\rangle$ with weights $(1-i)/2$ and $(1+i)/2$ [the Fourier expansion coefficients in Eq. (14)], respectively. This optical tomogram of the state $|\psi_2\rangle$ is a structure with two sinusoidal strands. Thus, a structure with two sinusoidal strands in the optical tomogram of the time-evolved state for an initial coherent state at $T_{\rm rev}/2$ is a signature of two-subpacket fractional revival. The quantum interference regions between the states $|i\alpha\rangle$ and $|-i\alpha\rangle$ are reflected in the optical tomogram of the state $|\psi_2\rangle$ at locations in the X_θ-θ plane, where the two sinusoidal strands intersect, showing a large oscillation in the optical tomogram.

The optical tomogram of the state $|\psi_3\rangle$, which is a state at the three-subpacket fractional revival, displays a structure with three sinusoidal strands [Fig. 1(c)]. Similarly, the optical tomogram of the state $|\psi_4\rangle$, which is a state at the four-subpacket fractional revival, plotted shows a structure with four sinusoidal strands [Fig. 1(d)]. We repeated the analysis for higher-order fractional revivals ($l > 4$) and found the general result that the optical tomogram of the time-evolved state at the l-subpacket fractional revival time shows a structure with l sinusoidal strands.

During the evolution of the coherent state $|\alpha\rangle$, the wave packet may also show the collapse phenomenon at specific instants of time $t = T_{\rm rev}/s$, where s is any irrational number [1]. The collapse phenomenon corresponds to the destruction of a wave packet during its evolution in a nonlinear medium due to the destructive interference of states comprising the wave packet [1,3,4,6,8,16]. The state at the instant of collapse is known as the collapsed state. At the instant of collapse the state $|\psi(t)\rangle$ is not a finite superposition of coherent states. It has been shown that such collapsed states of the fields are of great importance because of their high nonclassical nature and can give a large amount of entanglement when these states are split on a beam splitter with vacuum in the second input port [44]. To study the nature of the optical tomogram during the collapse of the wave packet, we plot the optical tomogram in Eq. (13) at collapse time $t = T_{\rm rev}/\sqrt{2}$. The optical tomogram at this instant is shown in Fig. 1(e). The sinusoidal strands are not visible in the optical tomogram for the collapsed state, which implies that the optical tomogram of a collapsed state is qualitatively different from that of the state at the instants of fractional revivals. Figure 1(f) shows the revival of the initial state at $t = T_{\rm rev}$. We can conclude that signatures of revivals and fractional revivals are captured in the optical tomogram of the time-evolved states. The optical tomogram at the instants of l-subpacket fractional revivals shows l sinusoidal strands for an initial coherent state, which has one strand in its optical tomogram.

B. Evolution of the m-photon-added coherent state

Here we consider the evolution of a nonclassical initial state, namely, an m-photon-added coherent state [45]

$$|\alpha,m\rangle = N_{\alpha,m}a^{\dagger m}|\alpha\rangle, \tag{19}$$

where $N_{\alpha,m}$ is the normalization constant and m is the number of photons added to the coherent field $|\alpha\rangle$. One of the states of this family, namely, the one-photon-added coherent state, has been experimentally produced by the parametric down-conversion process in a nonlinear crystal and the Wigner distribution of the state is reconstructed from the optical tomogram [46]. The Fock state expansion coefficient C_n in Eq. (7) for the m-photon-added coherent state is

$$C_n = \begin{cases} 0 & \text{if } n < m \\ \frac{e^{-|\alpha|^2/2}\alpha^{n-m}\sqrt{n!}}{\sqrt{m!L_m(-|\alpha|^2)(n-m)!}} & \text{if } n \geqslant m, \end{cases} \tag{20}$$

where L_m is the Laguerre polynomial of order m. The optical tomogram for the m-photon-added coherent state was investigated theoretically in [40]. The optical tomogram of the one-photon-added coherent state given in Fig. 2(a) displays a structure with a single sinusoidal strand. It shows a significant deviation of the intensity along the sinusoidal strand when compared with the optical tomogram of the coherent state given in Fig. 1(a). It is shown that the variation of the intensity becomes more pronounced as the value of m increases. This is due to the increase in nonclassicality of the m-photon-added coherent state with the increase in photon excitation number m [47,48]. The maximum intensity of the optical tomogram of the m-photon-added coherent state along the X_θ axis occurs at $X_\theta = \sqrt{2\langle N\rangle_m}\cos\delta$, where $\langle N\rangle_m$ is the mean photon number in the m-photon-added coherent state $|\alpha,m\rangle$.

The time evolution of the initial m-photon-added coherent state under the Kerr Hamiltonian shows revival and fractional revival at the same instants as in the case of the initial coherent state [49]. Substituting C_n in Eq. (10), we get the time evolution of the optical tomogram for the initial m-photon-added coherent state

$$\omega_{\alpha,m}(X_\theta,\theta,t) = \frac{e^{-|\alpha|^2}}{m!L_m(-|\alpha|^2)}\frac{e^{-X_\theta^2}}{\sqrt{\pi}} \times\left|\sum_{n=m}^{\infty}\frac{\alpha^{n-m}e^{-i\chi tn(n-1)}}{(n-m)!2^{n/2}}e^{-in\theta}H_n(X_\theta)\right|^2. \tag{21}$$

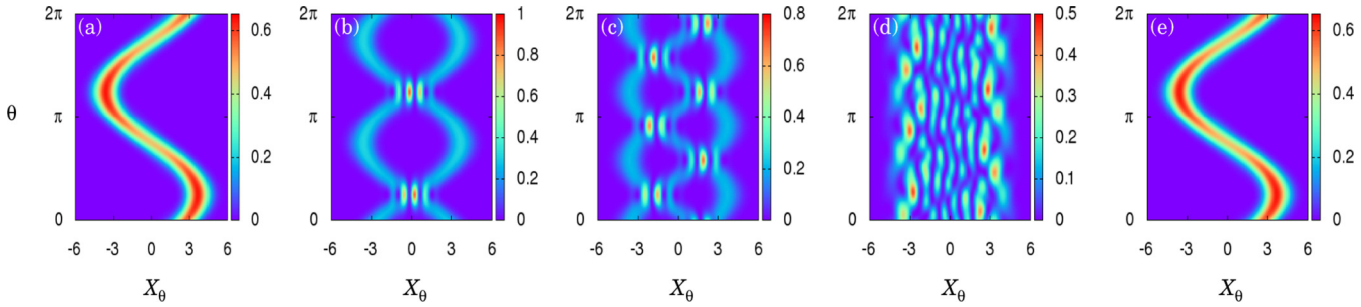

FIG. 2. (Color online) Time-evolved optical tomogram $\omega_{\alpha,1}(X_\theta,\theta,t)$ of the initial one-photon-added coherent state at (a) $t=0$, (b) $t=T_{\rm rev}/2$, (c) $t=T_{\rm rev}/3$, (d) $t=T_{\rm rev}/\sqrt{2}$, and (e) $t=T_{\rm rev}$, with field strength $|\alpha|^2=5$. At an l-subpacket fractional revival time $t=\pi/l\chi$, the optical tomogram of the state shows a structure with l sinusoidal strands. The structures with sinusoidal strands are completely absent in the optical tomogram for the collapsed state at time $t=T_{\rm rev}/\sqrt{2}$.

In Figs. 2(b)–2(e) we plot the optical tomograms $\omega_{\alpha,1}(X_\theta,\theta,t)$ for the evolution of the initial one-photon-added coherent state at different instants. Since the effect of photon addition to the coherent state $|\alpha\rangle$ is significant only for smaller field strengths, we choose $|\alpha|^2=5$ for the plots. Fourier expansion of the time-evolved state $|\psi(t)\rangle$ for an initial m-photon-added coherent state at the l-subpacket fractional revival time $t=\pi/l\chi$ can be written as

$$|\psi_l^{(m)}\rangle = \begin{cases} \sum_{r=0}^{l-1} f_r^{(o)} e^{-i2\pi rm/l}|\alpha e^{-i2\pi r/l},m\rangle & \text{if } l \text{ is odd} \\ \sum_{r=0}^{l-1} f_r^{(e)} e^{-i\pi m(2r-1)/l}|\alpha e^{-i\pi(2r-1)/l},m\rangle & \text{if } l \text{ is even.} \end{cases} \tag{22}$$

Each of the ket vectors appearing on the right-hand side of Eq. (22) is an m-photon-added coherent state and the state $|\psi_l^{(m)}\rangle$ is a superposition of l m-photon-added coherent states. The optical tomograms of the state $|\psi_l^{(m)}\rangle$ for an initial one-photon-added coherent state at two- and three-subpacket fractional revivals are shown in Figs. 2(b) and 2(c), respectively. The optical tomogram displays a structure with two sinusoidal strands at the two-subpacket fractional revival and is a structure with three sinusoidal strands at the three-subpacket fractional revival. The two sinusoidal strands in the optical tomogram of the state $|\psi_2^{(1)}\rangle$ correspond to the superposition of the states $|i\alpha,1\rangle$ and $|-i\alpha,1\rangle$. Similarly, the three sinusoidal strands in the optical tomogram of the state $|\psi_3^{(1)}\rangle$ correspond to the superposition of the states $|\alpha,1\rangle$, $|\alpha e^{-i2\pi/3},1\rangle$, and $|\alpha e^{i2\pi/3},1\rangle$. We repeated the analysis for higher values of photon excitation m and for higher-order fractional revivals ($l>3$) and found that at the instants of l-subpacket fractional revivals, the optical tomogram of the time-evolved state for an initial m-photon-added coherent state displays a structure with l sinusoidal strands. Figure 2(d) shows the optical tomogram of the time-evolved state for an initial one-photon-added coherent state at collapse time $t=T_{\rm rev}/\sqrt{2}$. In this case, the optical tomogram does not show any sinusoidal strand. Again, like in the case of an initial coherent state, the optical tomogram of the time-evolved state at time $t=T_{\rm rev}$ shows the revival of the initial one-photon-added coherent state. So far we have considered two types of initial states: coherent states and m-photon-added coherent states. These states are similar in the sense that both are single wave packets with a structure with a single sinusoidal strand in their optical tomograms. This is the reason for showing the same number of sinusoidal strands at the instants of fractional revivals for these two kinds of initial states. However, they are a completely different class of states because coherent states are classical states and the m-photon-added coherent state is a nonclassical state. This difference shows up in the intensity of sinusoidal strands in the optical tomogram. In the next section we consider superposed wave packets, which are different from the initial states considered so far.

C. Evolution of even and odd coherent states

Consider the evolution of even and odd coherent states [50], defined by

$$|\psi(0)\rangle_h = N_h[|\alpha\rangle + (-1)^h|-\alpha\rangle], \tag{23}$$

where $h=0$ and 1, respectively, and N_h is an appropriate normalization constant. The Fock state representation of the even (odd) coherent state contains only the even (odd) photon excitations. The revival and fractional revivals during the evolution of initial even and odd coherent states in a Kerr media have been discussed in detail [23]. It has been shown that [23] the time-evolved state at $t=kT_{\rm rev}/4$, where $k=1$, 2, and 3, is a rotated initial wave packet. Also, the l-subpacket fractional revival occurs at $t=jT_{\rm rev}/4l$, where $j=1,2,\ldots,4l-1$ for a given value of l (>1). Here j and $4l$ are mutually prime integers. The Fock state expansion coefficient C_n in Eq. (7) for the even and odd coherent states is given by

$$C_n = 2N_h e^{-|\alpha|^2/2}\frac{\alpha^n}{\sqrt{n!}}\delta_{[(n-h)/2],(n-h)/2}, \tag{24}$$

where δ is Kronecker delta function and $[x]$ is integer part of x. The symplectic tomography of even and odd coherent states was discussed in [29]. Inserting the value of the coefficient C_n in Eq. (10), we obtain the time-evolved optical tomogram for initial even and odd coherent states

$$\omega_h(X_\theta,\theta,t) = \frac{4N_h^2 e^{-|\alpha|^2}e^{-X_\theta^2}}{\sqrt{\pi}}\left|\sum_{n=0}^{\infty}\frac{\alpha^n e^{-i\chi tn(n-1)}}{n!2^{n/2}} \times e^{-in\theta}H_n(X_\theta)\delta_{[(n-h)/2],(n-h)/2}\right|^2. \tag{25}$$

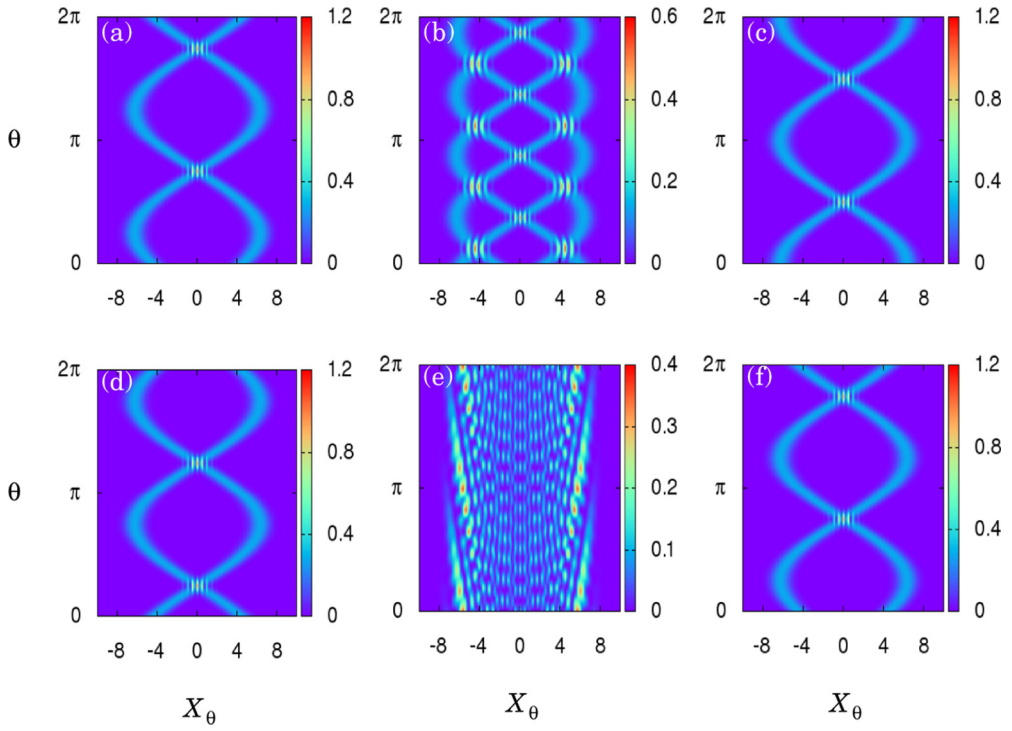

FIG. 3. (Color online) Time-evolved optical tomogram $\omega_0(X_\theta,\theta)$ of the initial even coherent state with field strength $|\alpha|^2 = 20$ at (a) $t = 0$, (b) $t = T_{\rm rev}/8$, (c) $t = T_{\rm rev}/4$, (d) $t = T_{\rm rev}/2$, (e) $t = T_{\rm rev}/\sqrt{2}$, and (f) $T_{\rm rev}$, respectively. At the instants of l-subpacket fractional revivals, the optical tomogram of the time-evolved state of the initial even coherent state displays a structure with $2l$ sinusoidal strands.

We focus on the evolution of an initial even coherent state $|\psi(0)\rangle_0$, but our analysis can be done for an initial odd coherent state as well. Figure 3(a) shows the optical tomogram of the even coherent state with $|\alpha|^2 = 20$, which displays a structure with two sinusoidal strands. In Figs. 3(b)–3(f) we plot the optical tomogram given in Eq. (25) at different instants during the evolution of the initial even coherent state ($h = 0$) in the medium. At the instants of rotated wave packets, the state is again a superposition of two coherent states. For example, at $t = T_{\rm rev}/4$ and $T_{\rm rev}/2$, Figs. 3(c) and 3(d) show the optical tomogram of rotated wave packets. The optical tomogram shows a structure with two sinusoidal strands, as expected. These tomograms are qualitatively different from the optical tomogram shown in Fig. 3(a). The locations of the sinusoidal strands, where the maximum intensity of the optical tomogram along the X_θ axis occurs, in these optical tomograms are shifted due to the phase-space rotation of the quantum states during the evolution of the initial even coherent state in the medium.

Figure 3(b) shows the optical tomogram of the time-evolved state at $T_{\rm rev}/8$, which corresponds to two-subpacket fractional revival. It displays a structure with four sinusoidal strands, which is a signature of two-subpacket fractional revival for the initial even coherent state. (Note that the optical tomogram of the initial even coherent state itself is a structure with two sinusoidal strands.) The time-evolved optical tomogram for initial even and odd coherent states is also analyzed at higher-order fractional revival times and we found that, at the instants of l-subpacket fractional revivals, the optical tomogram of the time-evolved state for the initial even and odd coherent state displays a structure with $2l$ sinusoidal strands. Figure 3(e) shows the optical tomogram of a collapsed state at time $t = T_{\rm rev}/\sqrt{2}$, which again confirms our result that sinusoidal strands are absent in the optical tomogram of the collapsed state. The optical tomogram of the time-evolved state at the revival time is shown in Fig. 3(f).

IV. EFFECT OF DECOHERENCE ON THE OPTICAL TOMOGRAM

So far we have analyzed the optical tomograms of pure quantum states undergoing unitary evolution in the Kerr medium. However, real optical nonlinearities are noisy and suffer various kinds of losses. This leads to decoherence of the quantum states prepared in an experiment. The effect of decoherence on the time-evolved states in a Kerr medium has been studied theoretically using quasiprobability distributions [51,52]. In this section we study the effect of environment-induced decoherence on the optical tomogram of the time-evolved state $|\psi(t)\rangle$ given in Eq. (9) at the instants of fractional revivals for the different initial states $|\psi(0)\rangle$ considered in the preceding section. Here we assume that the external environment consists of a collection of an infinite number of harmonic oscillators. Depending on the type of interaction between the single-mode field and the environment, the decoherence of the quantum state can occur at least in two ways: The first one is due to the photon absorption by the environment, also known as amplitude decay, and the second one is due to the phase damping. These two models are well described by master equations. Consider that the decoherence of the state $|\psi(t)\rangle$ starts at $\tau = 0$ and the density matrix of the

state at $\tau = 0$ is given by

$$\rho_t(\tau = 0) = |\psi(t)\rangle\langle\psi(t)|. \tag{26}$$

The evolution of this state under decoherence can be represented in the Fock basis as

$$\rho_t(\tau) = \sum_{n,n'=0}^{\infty} \rho_{t\,n,n'}(\tau)|n\rangle\langle n'|, \tag{27}$$

where the density-matrix elements $\rho_{t\,n,n'}(\tau)$ can be calculated using the appropriate master equations that describe the amplitude decay and phase damping of the state [53]. The interaction with the external environment leaves the system in a mixed state, that is, the state given in Eq. (27) is a mixed state for $\tau > 0$.

The optical tomogram of the state $\rho_t(\tau)$, using Eq. (2), takes the form

$$\omega(X_\theta,\theta,t;\tau) = \sum_{n,n'=0}^{\infty} \rho_{t\,n,n'}(\tau)\langle X_\theta,\theta|n\rangle\langle n'|X_\theta,\theta\rangle. \tag{28}$$

The expression (28) for the optical tomogram has been simplified to

$$\omega(X_\theta,\theta,t;\tau) = \frac{e^{-{X_\theta}^2}}{\sqrt{\pi}} \sum_{n,n'=0}^{\infty} \rho_{t\,n,n'}(\tau) \times \frac{H_n(X_\theta)H_{n'}(X_\theta)}{2^{(n+n')/2}\sqrt{n!n'!}} e^{-i(n-n')\theta}, \tag{29}$$

where we have used the quadrature representation $\langle X_\theta,\theta|n\rangle$ of the Fock state $|n\rangle$,

$$\langle X_\theta,\theta|n\rangle = \frac{1}{\pi^{1/4}2^{n/2}} \frac{e^{-{X_\theta}^2/2}}{\sqrt{n!}} H_n(X_\theta)e^{-in\theta}.$$

Evaluation of the optical tomogram $\omega(X_\theta,\theta,t;\tau)$ given in Eq. (29) involves the calculation of $\rho_{t\,n,n'}(\tau)$, which depends on the decoherence model. Next we calculate $\rho_{t\,n,n'}(\tau)$ for the amplitude decay model and the phase damping model.

A. Amplitude decay model

In this model the interaction of the single-mode field (mode a) with the environment modes e_j under the rotating-wave approximation can be described by the Hamiltonian

$$H_{\rm amp} = \sum_j \hbar\gamma(a{e_j}^\dagger + a^\dagger e_j), \tag{30}$$

where γ is the coupling strength of the mode a with the environment. In the Born-Markov approximation, the density matrix ρ_t in the interaction picture obeys the zero-temperature master equation

$$\frac{d\rho_t}{d\tau} = \gamma(2a\rho_t a^\dagger - a^\dagger a\rho_t - \rho_t a^\dagger a). \tag{31}$$

The matrix elements of ρ_t for an arbitrary initial state $\rho_t(\tau = 0)$ are calculated in the Fock basis using [54]

$$\rho_{t\,n,n'}(\tau) = e^{-\gamma\tau(n+n')} \sum_{r=0}^{\infty} \binom{n+r}{r}^{1/2} \binom{n'+r}{r}^{1/2} \times (1-e^{-2\gamma\tau})^r \rho_{t\,n,n'}(\tau = 0). \tag{32}$$

It should be noted that all the density-matrix elements $\rho_{t\,n,n'}(\tau)$ except those corresponding to $n = n' = 0$ decay exponentially to zero. In the long-time limit (i.e., $\tau \to \infty$) only the vacuum state will survive under amplitude decoherence, that is,

$$\rho_t(\tau \to \infty) = |0\rangle\langle 0|. \tag{33}$$

Using Eq. (32), we calculate the matrix elements $\rho_{t\,n,n'}(\tau)$ for the different initial states $|\psi(0)\rangle$ considered earlier as follows: (a) For the initial coherent state and the m-photon-added coherent state

$$\rho_{t\,n,n'}(\tau) = \frac{e^{-|\alpha|^2-\gamma\tau(n+n')}}{m!L_m(-|\alpha|^2)} \sum_{r=0}^{\infty} \binom{n+r}{r}^{1/2} \binom{n'+r}{r}^{1/2} \times (1-e^{-2\gamma\tau})^r \frac{\alpha^{n+r-m}\alpha^{*n'+r-m}\sqrt{(n+r)!(n'+r)!}}{(n+r-m)!(n'+r-m)!} \times e^{-i\chi t[(n+r)(n+r-1)-(n'+r)(n'+r-1)]} \tag{34}$$

($m = 0$ corresponds to the initial coherent state) and (b) for the initial even and odd coherent states

$$\rho_{t\,n,n'}(\tau) = 4N_h^2 e^{-|\alpha|^2} e^{-\gamma\tau(n+n')} \sum_{r=0}^{\infty} \binom{n+r}{r}^{1/2} \binom{n'+r}{r}^{1/2} \times (1-e^{-2\gamma\tau})^r \frac{\alpha^{n+r}\alpha^{*n'+r}}{\sqrt{(n+r)!(n'+r)!}} \times e^{-i\chi t[(n+r)(n+r-1)-(n'+r)(n'+r-1)]} \times \delta_{[(n+r-h)/2],((n+r-h)/2)} \times \delta_{[(n'+r-h)/2],[(n'+r-h)/2]}. \tag{35}$$

The optical tomograms of the initial m-photon-added coherent states and even and odd coherent states can be obtained using Eqs. (34) and (35), respectively, in Eq. (29). In the following, we analyze the amplitude damping of the state at the two-subpacket fractional revival time for different initial states. Figure 4 shows the optical tomograms of the state in the presence of amplitude damping at different times $\gamma\tau$ (scaled time) for the initial (a) coherent state ($m = 0$), (b) one-photon-added coherent state, and (c) even coherent state. The structures with sinusoidal strands are not lost when the interaction of the state with the environment is for a short duration of time (for example, when $\gamma\tau = 0.1$). The sinusoidal strands get close together and get distorted with an increase in time $\gamma\tau$ and they merge for large $\gamma\tau$. Figures 4(a) and 4(b) show the merging of two sinusoidal strands for the initial coherent state and the one-photon-added coherent state, respectively. Plots in Fig. 4(c) shows the merging of four sinusoidal strands for the initial even coherent state.

The merging of the sinusoidal strands with the increase in time $\gamma\tau$ is due to the decay of amplitude of the quantum state due to photon absorption by the environment. All the initial states considered above decay to the vacuum state in the long-time limit, i.e., when $\gamma\tau \to \infty$, and the corresponding optical tomogram is given by

$$\omega(X_\theta,\theta,t;\tau \to \infty) = \frac{1}{\sqrt{\pi}} e^{-X_\theta^2}. \tag{36}$$

The above optical tomogram $\omega(X_\theta,\theta,t;\tau \to \infty)$ is a structure with a single straight strand in the X_θ-θ plane, which the last

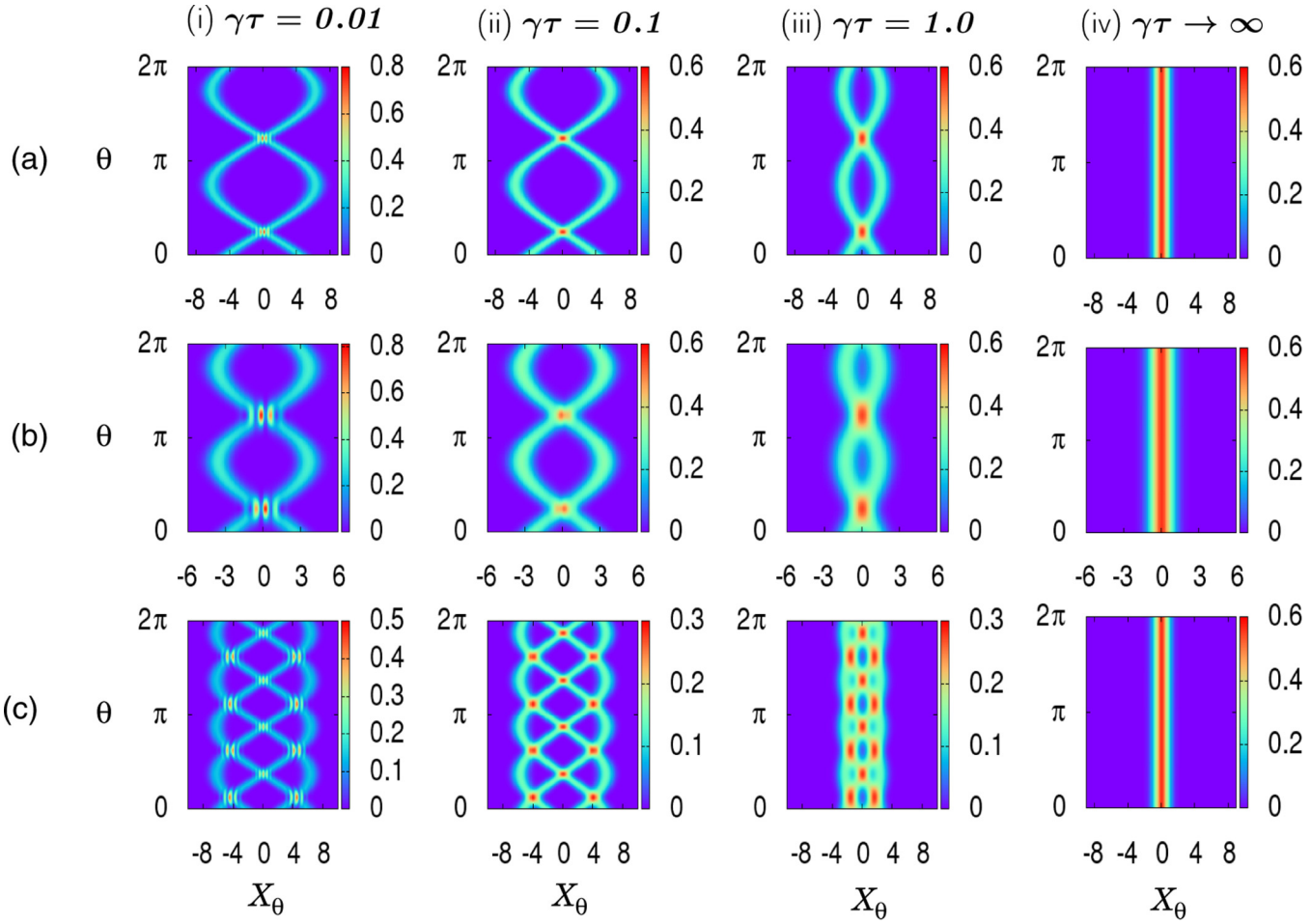

FIG. 4. (Color online) Optical tomograms of the states at two-subpacket fractional revival time in the presence of amplitude damping for an initial (a) coherent state with $|\alpha|^2 = 20$, (b) one-photon-added coherent state with $|\alpha|^2 = 5$, and (c) even coherent state with $|\alpha|^2 = 20$ at (i) $\gamma\tau = 0.01$, (ii) $\gamma\tau = 0.1$, (iii) $\gamma\tau = 1.0$, and (iv) $\gamma\tau \to \infty$.

column of Fig. 4 confirms. Another important fact is that the oscillations in the optical tomogram in the interference regions of the sinusoidal strands decrease with the increase in decoherence time $\gamma\tau$, which can be observed in Fig. 4. We repeated the analysis described above for the states at the instants of higher-order fractional revivals and found similar results.

B. Phase damping model

In the phase damping model, the interaction between the system (represented by the mode a) and the environment modes e_j can be modeled by the Hamiltonian [53]

$$H_{\rm ph} = \sum_j \hbar\kappa (A e_j^\dagger + A^\dagger e_j), \tag{37}$$

where $A = a^\dagger a$ and κ is the coupling constant. In this case, the interaction with the environment causes no loss of energy of the system but the information about the relative phase of the energy eigenstates is lost. The Markovian dynamics of the state ρ_t is described by the zero-temperature master equation

$$\frac{d\rho_t}{d\tau} = \kappa(2A\rho_t A^\dagger - A^\dagger A\rho_t - \rho_t A^\dagger A). \tag{38}$$

The matrix elements of ρ_t for an arbitrary initial state $\rho_t(\tau = 0)$ are given by [53]

$$\rho_{t\,n,n'} = \exp[-\kappa(n-n')^2\tau]\rho_{t\,n,n'}(\tau = 0). \tag{39}$$

Here the diagonal matrix elements do not decay due to phase damping. Using Eq. (39) we calculate the matrix elements of $\rho_t(\tau)$ in the presence of phase damping for different initial states as follows: (a) For the initial coherent state and m-photon-added coherent states

$$\rho_{t\,n,n'}(\tau) = \frac{e^{-(n-n')^2\kappa\tau} e^{-|\alpha|^2} \alpha^{n-m} \alpha^{*n'-m} \sqrt{n!n'!}}{m! L_m(-|\alpha|^2)(n-m)!(n'-m)!} \times e^{-i\chi t[n(n-1)-n'(n'-1)]} \tag{40}$$

($m = 0$ corresponds to the initial coherent state) and (b) for the initial even and odd coherent states

$$\rho_{t\,n,n'}(\tau) = \frac{4N_h^2 e^{-(n-n')^2\kappa\tau - |\alpha|^2} \alpha^n \alpha^{*n'}}{\sqrt{n!n'!}} e^{-i\chi t[n(n-1)-n'(n'-1)]} \times \delta_{[(n-h)/2],(n-h)/2} \delta_{[(n'-h)/2],(n'-h)/2}. \tag{41}$$

Substituting Eqs. (40) and (41) in Eq. (29) gives the optical tomogram of the time-evolved state $|\psi(t)\rangle$ under phase

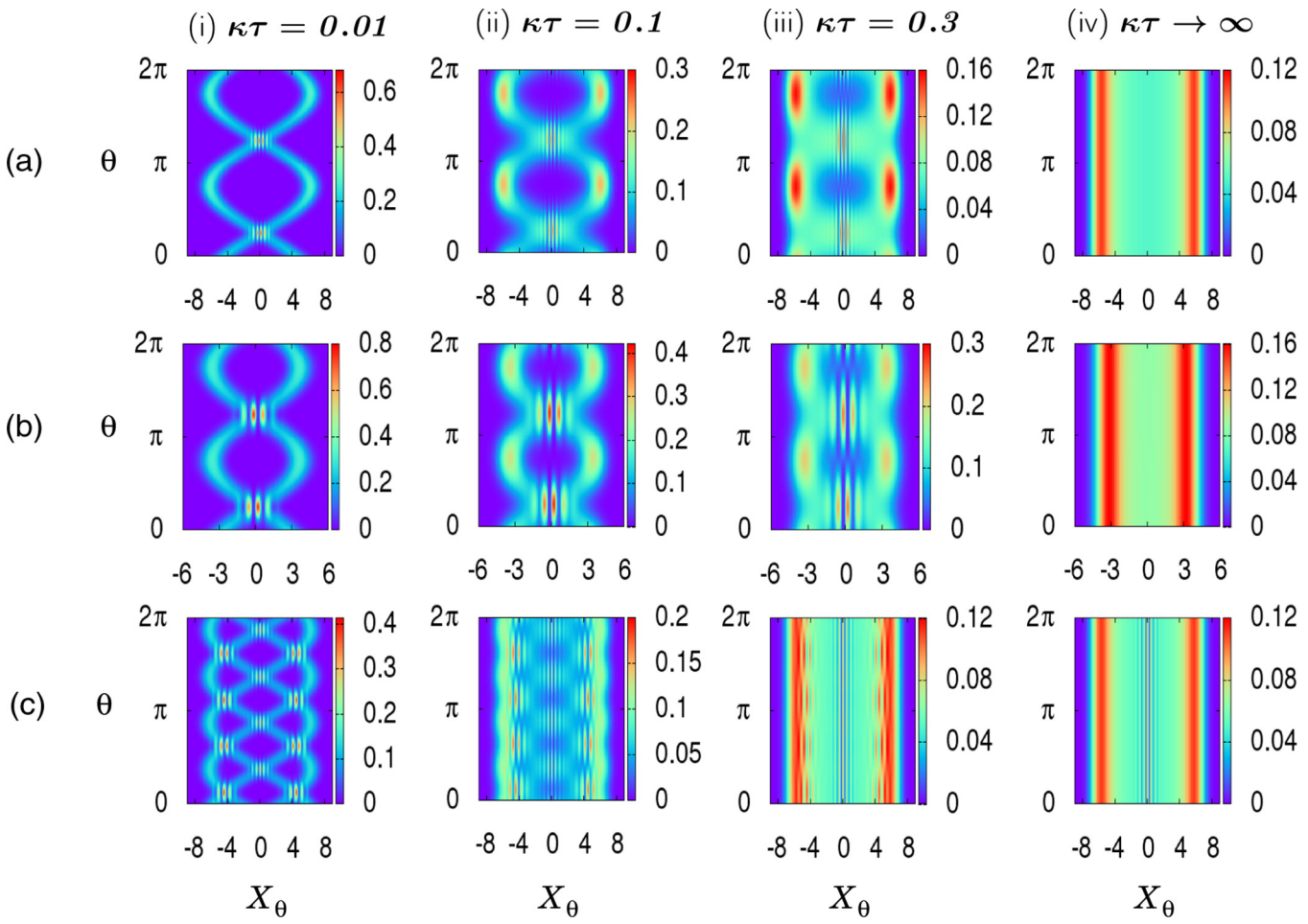

FIG. 5. (Color online) Optical tomograms of the states at a two-subpacket fractional revival time in the presence of phase damping for an initial (a) coherent state with $|\alpha|^2 = 20$, (b) one-photon-added coherent state with $|\alpha|^2 = 5$, and (c) even coherent state with $|\alpha|^2 = 20$ at (i) $\kappa\tau = 0.01$, (ii) $\kappa\tau = 0.1$, (iii) $\kappa\tau = 0.3$, and (ii) $\kappa\tau \to \infty$.

damping for the initial m-photon-added coherent state and for the even and odd coherent states, respectively. In the following we consider the phase damping of the state at the two-subpacket fractional revival time for different initial states. Figure 5 shows the optical tomograms of the state in the presence of phase damping at different times $\kappa\tau$ (scaled time) for the initial (a) coherent state ($m = 0$), (b) one-photon-added coherent state, and (c) even coherent state. In contrast to the amplitude damping, the phase damping shows a faster decay of the sinusoidal strands in the optical tomogram of the states. The sinusoidal strands in the optical tomogram of the state retain their structure only for a short time $\kappa\tau$. The faster decay of the state is very noticeable in the case of an initial even coherent state; this aspect is displayed in Fig. 5(c).

In the long-time limit $\rho_t(\tau \to \infty)$, the optical tomograms $\omega(X_\theta,\theta,t;\tau \to \infty)$ of different initial states are as follows: (a) For the initial coherent state and m-photon-added coherent states

$$\omega(X_\theta,\theta,t;\tau \to \infty) = \frac{e^{-X_\theta{}^2-|\alpha|^2}}{\sqrt{\pi}m!L_m(-|\alpha|^2)} \times \sum_{n=m}^{\infty} \frac{|\alpha|^{2(n-m)}H_n^2(X_\theta)}{2^n[(n-m)!]^2} \quad (42)$$

($m = 0$ corresponds to the initial coherent state) and (b) for even and odd coherent states

$$\omega(X_\theta,\theta,t;\tau \to \infty) = \frac{4N_h^2 e^{-X_\theta{}^2-|\alpha|^2}}{\sqrt{\pi}} \sum_{n=0}^{\infty} \frac{|\alpha|^{2n}H_n^2(X_\theta)}{2^n(n!)^2} \times \delta_{[(n-h)/2],(n-h)/2}. \quad (43)$$

Both of the above tomograms are independent of the phase θ; this is displayed in the last column of Fig. 5. We have repeated the above analysis for higher-order fractional revivals and found similar results. The optical tomogram of the states, in the long-time scales, shows a completely different structure for amplitude damping and phase damping models of the decoherence. This can be used to understand the type of interaction the system is having with its environment.

V. CONCLUSION

We have studied the optical tomograms of different kinds of wave packets evolving in a Kerr medium. The exact analytical expression for the optical tomogram of the quantum states at any instant during the evolution of a generic initial wave packet is derived in terms of Hermite polynomials. The time

evolution of the optical tomogram is analyzed for three specific initial states: a coherent state, an m-photon-added coherent state, and even and odd coherent states. We have shown that the signatures of revival and fractional revivals are captured in the optical tomograms of the quantum states. The optical tomogram of the time-evolved state at the instants of fractional revivals shows structures with sinusoidal strands. In general, the number of sinusoidal strands in the optical tomogram of the time-evolved state at l-subpacket fractional revivals is l times the number of sinusoidal strands present in the optical tomogram of the initial state considered. There are no sinusoidal strands present when the initial state collapses during the evolution. Interactions of the system with its environment are inevitable in a real experimental setting and we found the manifestations of decoherence directly in the optical tomogram. The results obtained in this paper may be very useful for the experimental characterization of revivals and fractional revivals for the following reasons. (i) We have shown the signatures of fractional revivals directly in the optical tomogram of the states. There is no need to reconstruct the density matrix or the quasiprobability distribution from the experimentally obtained optical tomogram to study fractional revivals, so there is no need to be concerned about the error that can accumulate during the reconstruction process. (ii) The analytical results obtained can be used to verify and compare the optical tomograms generated in a homodyne measurement. (iii) The theoretical results on decoherence can be used to find out how much the decoherence models really capture the effects of environmental interactions in an actual experimental setting.

[1] R. W. Robinett, Phys. Rep. **392**, 1 (2004).
[2] I. S. Averbukh and N. F. Perelman, Phys. Lett. A **139**, 449 (1989).
[3] G. Rempe, H. Walther, and N. Klein, Phys. Rev. Lett. **58**, 353 (1987).
[4] J. A. Yeazell, M. Mallalieu, and C. R. Stroud, Jr., Phys. Rev. Lett. **64**, 2007 (1990).
[5] J. A. Yeazell and C. R. Stroud, Jr., Phys. Rev. A **43**, 5153 (1991).
[6] D. R. Meacher, P. E. Meyler, I. G. Hughes, and P. Ewart, J. Phys. B **24**, L63 (1991).
[7] M. J. J. Vrakking, D. M. Villeneuve, and A. Stolow, Phys. Rev. A **54**, R37 (1996).
[8] M. Greiner, O. Mandel, T. W. Hansch, and I. Bloch, Nature (London) **419**, 51 (2002).
[9] D. N. Matsukevich, T. Chaneliére, S. D. Jenkins, S.-Y. Lan, T. A. B. Kennedy, and A. Kuzmich, Phys. Rev. Lett. **96**, 033601 (2006).
[10] B. Yurke and D. Stoler, Phys. Rev. Lett. **57**, 13 (1986).
[11] A. Miranowicz, R. Tanaś, and S. Kielich, Quantum Opt. **2**, 253 (1990).
[12] M. Paprzycka and R. Tanaś, Quantum Opt. **4**, 331 (1992).
[13] K. Tara, G. S. Agarwal, and S. Chaturvedi, Phys. Rev. A **47**, 5024 (1993).
[14] N. J. Cerf, A. Ipe, and X. Rottenberg, Phys. Rev. Lett. **85**, 1754 (2000).
[15] E. A. Shapiro, M. Spanner, and M. Y. Ivanov, Phys. Rev. Lett. **91**, 237901 (2003).
[16] G. Kirchmair, B. Vlastakis, Z. Leghtas, S. E. Nigg, H. Paik, E. Ginossar, M. Mirrahimi, L. Frunzio, S. M. Girvin, and R. J. Schoelkopf, Nature (London) **495**, 205 (2013).
[17] I. Jex and A. Orłowski, J. Mod. Opt. **41**, 2301 (1994).
[18] J. A. Vaccaro and A. Orłowski, Phys. Rev. A **51**, 4172 (1995).
[19] A. Miranowicz, J. Bajer, M. R. B. Wahiddin, and N. Imoto, J. Phys. A: Math. Gen. **34**, 3887 (2001).
[20] C. Sudheesh, S. Lakshmibala, and V. Balakrishnan, Phys. Lett. A **329**, 14 (2004).
[21] E. Romera and F. de los Santos, Phys. Rev. Lett. **99**, 263601 (2007).
[22] E. Romera and F. de los Santos, Phys. Rev. A **78**, 013837 (2008).
[23] M. Rohith and C. Sudheesh, J. Phys. B **47**, 045504 (2014).
[24] U. Leonhardt, *Measuring the Quantum State of Light* (Cambridge University Press, Cambridge, 1997).
[25] K. Vogel and H. Risken, Phys. Rev. A **40**, 2847 (1989).
[26] S. Mancini, V. I. Man'ko, and P. Tombesi, Quantum Semiclass. Opt. **7**, 615 (1995).
[27] G. M. D'Ariano, S. Mancini, V. I. Man'ko, and P. Tombesi, Quantum Semiclass. Opt. **8**, 1017 (1996).
[28] O. Man'ko and V. I. Man'ko, J. Russ. Laser Res. **18**, 407 (1997).
[29] S. Mancini, V. I. Man'ko, and P. Tombesi, Phys. Lett. A **213**, 1 (1996).
[30] V. I. Man'ko and R. Vilela Mendes, Phys. Lett. A **263**, 53 (1999).
[31] V. I. Man'ko, G. Marmo, A. Simoni, A. Stern, and F. Ventriglia, Phys. Lett. A **343**, 251 (2005).
[32] V. I. Man'ko, G. Marmo, A. Simoni, A. Stern, E. C. G. Sudarshan, and F. Ventriglia, Phys. Lett. A **351**, 1 (2006).
[33] A. Ibort, V. I. Man'ko, G. Marmo, A. Simoni, and F. Ventriglia, Phys. Scr. **79**, 065013 (2009).
[34] D. T. Smithey, M. Beck, M. G. Raymer, and A. Faridani, Phys. Rev. Lett. **70**, 1244 (1993).
[35] A. I. Lvovsky and M. G. Reymer, Rev. Mod. Phys. **81**, 299 (2009).
[36] M. Bellini, A. S. Coelho, S. N. Filippov, V. I. Man'ko, and A. Zavatta, Phys. Rev. A **85**, 052129 (2012).
[37] G. J. Milburn, Phys. Rev. A **33**, 674 (1986).
[38] M. Kitagawa and Y. Yamamoto, Phys. Rev. A **34**, 3974 (1986).
[39] S. N. Filippov and V. I. Man'ko, Phys. Scr. **83**, 058101 (2011).
[40] Y. A. Korennoy and V. I. Man'ko, Phys. Rev. A **83**, 053817 (2011).
[41] A. Miranowicz, M. Paprzycka, A. Pathak, and F. Nori, Phys. Rev. A **89**, 033812 (2014).
[42] M. Rohith and C. Sudheesh, arXiv:1505.02698.
[43] S. M. Barnett and P. M. Radmore, *Methods in Theoretical Quantum Optics* (Oxford University Press, Oxford, 1997).
[44] M. Rohith, R. Rajeev, and C. Sudheesh, arXiv:1409.2643.
[45] G. S. Agarwal and K. Tara, Phys. Rev. A **43**, 492 (1991).
[46] A. Zavatta, S. Viciani, and M. Bellini, Science **306**, 660 (2004).
[47] C. Sudheesh, S. Lakshmibala, and V. Balakrishnan, J. Opt. B **7**, S728 (2005).

[48] A. R. Usha Devi, R. Prabhu, and M. S. Uma, Eur. Phys. J. D **40**, 133 (2006).
[49] C. Sudheesh, S. Lakshmibala, and V. Balakrishnan, Europhys. Lett. **71**, 744 (2005).
[50] V. V. Dodonov, I. A. Malkin, and V. I. Man'ko, Physica **72**, 597 (1974).
[51] G. J. Milburn and C. A. Holmes, Phys. Rev. Lett. **56**, 2237 (1986).
[52] D. J. Daniel and G. J. Milburn, Phys. Rev. A **39**, 4628 (1989).
[53] C. W. Gardiner, *Quantum Noise* (Springer, Berlin, 1991).
[54] A. Biswas and G. S. Agarwal, Phys. Rev. A **75**, 032104 (2007).